Desalination and Water Treatment
www.deswater.com

doi: 10.5004/dwt.2021.27631

234 (2021) 158–173
September

Sorption of phenol from aqueous solution onto soil-agro blend by diffusion modeling

Busetty Subramanyam

School of Civil Engineering, SASTRA Deemed University, Thanjavur, India 613401, emails: subramanyamjy@gmail.com/subramanyam@civil.sastra.edu (B. Subramanyam)

Received 21 January 2021; Accepted 17 July 2021

ABSTRACT

In this study, the inorganic–organic composite combination had its impact on kinetics, diffusion, equilibrium, and the mechanism of phenol uptake. The soils locally available and the agro-based composite were prepared and applied to phenol adsorption at various concentrations. The values obtained from the external mass transmission coefficients vary between 1.04×10^{-6} cm/s and 1.76×10^{-4} cm/s. When comparing Adhanur-black gram husk (Ar-BGH) and Kalathur-rice husk (Kr-RH) adsorbents in this study with external mass coefficients of every individual adsorber, the resistance is lower than the resistance of other adsorbents like Kalathur (Kr) soil, Adhanur (Ar) soil and Kalathur-black gram husk (Kr-BGH). Parameters of the intraparticle rate have been evaluated for the diffusion of the intraparticle. The gradual increase of '*K*' with an increase in C_0 is observed. The values of *A* and *B* for phenol adsorption were evaluated on two natural and soil-agro blends and the R^2 correlation coefficient was identified as 0.98. The linearity of the '$t^{0.5}$' plots means that the chemical reaction and diffusion adsorption are combined. They are the major rate control step throughout the adsorption.

Keywords: Adsorption; Kinetics; Diffusion; Equilibrium; Modeling; Phenol

1. Introduction

As a common pollutant, phenol and its derivatives are produced by the majority of industries, including pharmaceuticals, coal conversion, dying, textiles, and wood. phenol and its derivatives are harmful to the environment at low concentrations. The Food and Drug Administration (FDA) and Indian Standard Drinking Water have determined that the phenol concentration in bottled drinking water should not exceed 0.001 mg/L [1]. The removal of phenol and its derivatives by various adsorbents has been the subject of several recent research papers. Also, there has been an increasing interest in utilizing natural soils for the removal of phenol and phenolic compounds from aqueous solutions [2–8]. In recent years, there has been increasing interest in utilizing natural soil/clay minerals such as montmorillonite, kaolinite, and illite for the removal of toxic metals and some organic pollutants from aqueous solutions [9–12]. Because of the abundance of soil/clay on most continents and its low cost, it is an excellent candidate as an adsorbent for the removal of many pollutants from waste. The suitability of using natural bentonite (mainly montmorillonite) for the sorption of phenol from an aqueous solution has been studied by Banat et al. [13]. In this work, the phenol removal by raw clay (RCG) and calcined one at 1,000°C (CCG) was investigated. The kinetics and isotherms experiments were also studied at pH = 4. The results indicated that the phenol adsorption reached equilibrium within 3 h, and the removal of phenol was enhanced at the same temperature by CCG (2.932 mg/g) adsorbent, compared to RCG (1.640 mg/g) due to the removal of organic matter by heat treatment, and an increase in adsorption temperature, indicating the endothermic process [14]. Surfactant-modified clays also allow for the simultaneous removal of organic contaminants and heavy

metals. Montmorillonite modified with carboxy decyl triethyl ammonium bromide (CDTEA-Br) showed promise for the adsorption of both Pb(II) and chlorobenzene [15]. The adsorption capacity of natural kaolin has been significantly increased by modification (19.2 and 5.1 mg/g for Cu(II) and phenol, respectively) up to 38.5 mg/g for Cu(II), 91.5 mg/g for phenol, and 51.8 mg/g for o-xylene [16]. This work focused on the thermal modification of a commercial layered double hydroxide (LDH) clay and its subsequent effectiveness as an adsorbent in the removal of phenol from wastewater. The Brunauer–Emmett–Teller surface area increased by 233% upon calcination at 500°C. The highest phenol removal (85%) was observed in the clay calcined at 500°C compared to 10% for the neat clay. Optimization studies revealed a maximum adsorption capacity of 12 mg/g at an adsorbent loading of 10 g/L at pH 7. The equilibrium data were best fitted to the Freundlich isotherm model which describes heterogeneous adsorption. The adsorption kinetics followed a pseudo-second-order kinetic model [17]. Some of the main LDH properties that give rise to good adsorption properties include surface area, crystallinity, composition, and surface chemistry [18]. In recent years, the use of agro-waste for the preparation of biosorbent in water and wastewater treatment has been reported in the literature [19–22].

The adsorption capacity of agro-waste depends on the ion-exchange, hydrogen bonding, and chelation capacity of the materials. The adsorption of pollutants onto the agro-waste can be divided into four processes, namely (i) diffusion from bulk solution across the liquid film surrounding the biomaterial particles (film diffusion or external mass transfer); (ii) adsorption onto adsorbent sites on the surface of the biomaterial particles (surface adsorption); (iii) internal diffusion into the biomaterial particles (intraparticle or internal mass transfer diffusion) and (iv) adsorption of pollutants species on the walls of the pores of the biomaterial particles [19,23,24]. Thomas and Weber et al. [25], studied heat and mass transfer processes in adsorption-packed bed using silica gel. They concluded that the performance of a silica gel-packed bed is controlled by the conductive thermal resistance when the Fourier number of the adsorbent–adsorbate layer (F_o) is less than 1.0. The convective resistance (i.e., external resistance) dominates the bed performance when the dimensionless temperature ratio (Θ) of adsorption silica gel packed bed is more than 0.2. In this study, NaOH treated pine (NTP) and magnetite-pine composite (NTP-NC) were prepared and applied for Cr(VI) adsorption, the impact of the diffusion, equilibrium, and Cr(VI) uptake mechanism was determined. The intraparticle diffusion coefficient, D_i, wherein the range of 10^{-5} to 10^{-13} cm^2/s indicating that intraparticle diffusion occurred in a chemisorption-controlled process. This was confirmed by the good fit of the chemisorption–diffusion model with the experimental data. Film diffusion was found to be active in the mechanism of Cr(VI) uptake by NTP, but pore diffusion was active for NTP-NC [26)]. Agnes et al. [27] studied the effect of a commercial resin to adsorb four parabens used as probe molecules. With such an aim, a heterogeneous three-parameter intraparticle diffusion model was formulated, and its numerical solution was fitted to time-dependent concentration data by minimizing the sum of squared residuals. Additionally, the order of magnitude of pore diffusivity obtained in this work is in accordance with the one predicted by Wilke–Chang correlation and is inversely proportional to the van der Waals volume raised to the power 0.53 in close agreement with the literature. The authors evaluated the interaction in the water of magnetite-coated pinecone biomass with As(III) as an efficient adsorbent. Adsorption trials have shown that As(III) is optimally adsorbed at pH 8. Fe_3O_4: pinecone for As(III) with a capacity of 13.86 mg/g for removal was optimal 2.0 g Fe_3O_4:1.5 g pinecone. The second-order pseudo-model was calculated to be 23.78 kJ/mol for the kinetic data that best fitted the activation energy. Dubinin–Radushkevich means free energy values that suggest an anion-exchange process, while Langmuir isotherm best describes balance data [28]. The authors produced the effect of the magnetic pinecone (MNP-PCP) on the removal capacity of Cr(VI) via Fe^{2+}/Fe^{3+} co-precipitation on different weights. At every solution pH 3, the composite with 1.5 g pine has extracted more Cr(VI), which has leached Fe(III) to less than 0.01 mg/L. The capacity of Langmuir monolayers was observed to be 15.24 mg/g at 26°C, while free energy ranged from 15.80 to 16.80 kJ/mol from Dubinin–Radushkevich and suggested a ligand–ion-exchange mechanism [29].

Agro-residue refers to a wide variety of wastes obtained from agricultural products-grains, pulses, fruits, vegetables, and spices, generated from various parts of the plants (stem, root, fruit, leaf, flowers, etc). The initial selection of the agro-wastes for the study was carried out based on five parameters (namely 1. Seasonal production, 2. Non-acidic character, 3. Essentiality for other usages, 4. Agro-waste production in terms of volume/yield and 5. Cost-effectiveness). Certain agro-wastes were deliberately ignored by the author because of their infeasibility, inconvenience, or unavailability. Table 1 presents synoptic evaluation criteria and results obtained thereof.

The film diffusion model has been used by several researchers to determine external mass transfer coefficients for the sorption of phenol. The intraparticle mass transfer coefficient has been studied by Pholosi et al. [30], who reported that the intraparticle mass transfer coefficient for dinitro-o-sec-butyl phenol varies with the initial concentration and with the diameter of the particle. Distribution profiles in branched pore models for gas adsorption are reported by Do [31], Hu [32], and Hu et al. [33]. A solid-phase diffusion model was developed by Mathews and Weber [34], based on finite difference approximations for any arbitrary isotherm and extended the model to multi-component systems. Weber and Morris [35], Crank [36], McKay et al. [37]

Table 1
Proximate analyses of raw agro-wastes

Name	Moisture content	Volatile matter	Ash content	Fixed carbon
Rice husk (RH)	7.80	53.20	25.20	13.80
Green gram husk (GGH)	4.25	75.00	8.70	12.05
Black gram husk (BGH)	8.00	70.60	5.50	15.90

in their studies developed another type of single resistance model based on intraparticle diffusion. The model correlates the linear relationship between the sorption uptake (q_t) and the square root of time ($t^{0.5}$).

The current study focuses on an important aspect of pore diffusion and the calculation of pore diffusion coefficients from batch mode experimental data. The pore diffusion coefficient of a model can be calculated by fitting it to experimental data. However, for nonlinear systems, the experimental data fitting process is often complicated by the need to solve the model equations numerically [32,33]. The current study investigates the feasibility of using a simple kinetic model to calculate external mass transfer coefficients from batch kinetic data as well as numerical methods. The adsorption of a solute onto the surface of an adsorbent is investigated in this study. Adsorption of solute onto the surface of the adsorbent is assumed to be rapid in the current study, so it is not considered the rate-limiting step. Whereas mass transfer of a solute from the bulk solution to the particle surface (external mass transfer) and internal mass transfer within the particle (pore diffusion or solid diffusion) were thought to be rate-limiting steps. The pore diffusion model assumes that the aqueous solution first diffuses into the pores, where phenol molecules are adsorbed onto the internal surface of the adsorbents.

1.2. Diffusion based models

1.2.1. Sorption diffusion models

Adsorption kinetics are determined by the forces and interactions that exist between individual atoms, ions, or molecules of adsorbate and the surface or interface. Equilibrium studies can provide fundamental information for modeling the adsorption of adsorbate onto an adsorbent. The adsorption mechanism of phenol, which has large molecules and a long contact time to equilibrium, is mostly diffusion control. Diffusion adsorption is typically governed by an external film resistance and/or internal diffusion mass transport or intraparticle diffusion. The diffusion process consists of four steps of migration/transport adsorbate to move from the bulk fluid phasing. Whereas there are three processes for adsorption on the particle's outer surface, which are normally extremely minor and ignored in comparison to adsorbed on the surface of the pores.

The following mass-transfer mechanisms may be involved during adsorption:

1.2.2. Bulk transport

Which is also referred to as the transport of adsorbate in the solution phase to the vicinity of the particle. In a well-agitated batch system, bulk mass transfer is so rapid that is not considered as the rate-limiting step.

1.2.3. Film transport

Which is referred to as diffusion of the adsorbate through a film which causes a resistance to mass transfer at the surface of the adsorbent particle.

1.2.4. Intraparticle transport

Which refers to the mass diffusion adsorbate within the adsorbent particle. It involves two-step mechanisms for diffusion adsorbate within the adsorbent particle: pore diffusion and surface diffusion.

The overall rate of the adsorption process will be controlled by the slowest step mechanisms, which is film transport (external diffusion)/intraparticle transport (internal diffusion). These two rate-limiting steps had been developed by several workers.

1.2.5. Calculation of the external mass transfer coefficient

The adsorption rate is represented as follows:

$$\frac{dC_t}{dt} = -K_f S_A \left(C_t - C_s\right) \tag{1}$$

with initial conditions:

$$\text{At } t = 0;\ C_t = C_0 \tag{2}$$

The particle is assumed to be spherical, external surface area per unit volume of solution S_A can be calculated as follows:

$$S_A = \frac{A_s}{V} = \frac{6M_s}{d_p \rho_b} \tag{3}$$

Integrating the Eqs. (2) & (3) and applying boundary conditions (0, C_0) to (t, C_t):

$$\ln\left(\frac{C_t}{C_0}\right) = -K_f S_A t \tag{4}$$

A plot of $\ln(C_t/C_0)$ vs. t gives a straight line of slope K_f:S_A. Knowing S_A, the value of the external diffusion coefficient (K_f) can be estimated.

1.2.6. Intraparticle diffusion control

The mathematical theory of diffusion in isotropic substances is based on the hypothesis that the rate of transfer of diffusing substance through the unit area of section (F) is propositional to the concentration gradient measured normal to the section. This is given by Fick's first law of diffusion:

$$F = -D\frac{\partial C}{\partial x} \tag{5}$$

The fundamental equation of diffusion, where there is a concentration gradient along the 'x' axis is given by Fick's second law of diffusion:

$$\frac{\partial C}{\partial t} = D\frac{\partial^2 C}{\partial x^2} \tag{6}$$

Boyd et al. [38] constructed a mathematical derivation based on the aforementioned two diffusion laws (cited by Crank [39]; Srivastava et al. [40]), which was valid under the experimental circumstances utilized. The simultaneous solution of a collection of differential and algebraic equations leads to:

$$\frac{q_t}{q_e}=6\left(\frac{Dt}{R^2}\right)^{0.5}\left\{\pi^{-0.5}+2\sum_{n=1}^{\infty}\text{ierfc}\frac{nR}{Dt^{0.5}}\frac{nR}{Dt^{0.5}}\right\}-3\frac{Dt}{R^2} \tag{7}$$

where D can be replaced by the diffusion coefficient D_f:

$$\frac{q_t}{q_e}=6\left(\frac{D_f t}{\pi R^2}\right)^{0.5} t^{0.5} \tag{8}$$

Eq. (7) can be written as follows:

$$F(t)=\frac{q_t}{q_e}=1-\frac{6}{\pi^2}\sum_{n=1}^{\infty}\frac{1}{n^2}\exp\left(-\frac{D_i\pi^2n^2t}{r^2}\right) \tag{9}$$

Eq. (9) converges asymptotically over time since the higher terms of the summation become small and are negligible, can be rewritten as:

$$1-\frac{q_t}{q_e}=\frac{6}{\pi^2}\exp\left(-\frac{D_i\pi^2z^2t}{r^2}\right)t \tag{10}$$

and

$$1-\frac{q_t}{q_e}=\frac{6}{\pi^2}\exp\left(-k'\right)t \tag{11}$$

k' is the overall rate constant as:

$$k'=-\frac{D_i\pi^2z^2t}{r^2} \tag{12}$$

Taking logarithm on both sides of Eq. (11):

$$\ln\left(1-\frac{q_t}{q_e}\right)=\ln\frac{6}{\pi^2}-k't \tag{13}$$

A plot of '$\ln(1-q_t/q_e)$' vs. 't' gives a straight line of slope 'k' and using Eq. (12) internal diffusion coefficient (D_i) can be calculated.

2. Materials and methodology

2.1. Materials

The soils used in the study were from the Kalathur soil (Kr) series and Adhanur soil (Ar) series at Thanjavur, Tamil Nadu, and India. The Kalathur soil series consists of very dark grey, brown, very deep, calcareous, fine-textured Cauvery River alluvium. The soil is classified as Oxisols. The Adhanur soil series consists of grayish brown, fine loamy, very deep, and strongly calcareous. The soil is classified as Alfisols. Vertisols are weathered soils and are poorly drained, with relatively low native fertility. Vertisols consist mainly of quartz, kaolinite, oxides, and organic matter. They appear structureless and have the feel of a loamy texture. While some are loamy or even coarser textured, many have a fine or very fine particle-size class, but the clay is aggregated in a strong grade of fine and very fine granular structure. Alfisols have an ochric epipedon, an argillic horizon, and moderate to high base saturation and in which water is moderately drained.

2.2. Selection and characterization of the adsorbent samples

2.2.1. Soil samples

Soil samples were collected and dried overnight in an electric at 105°C, then crushed (24 h in a ball mill) and sieving (100–635 (0.15–0.02 mm) SIEVE NO ASTM E11-87), to obtain the particles having an average diameter of 0.05 mm. The resulting material was dried, desiccated, and stored in an air-tight container for further examination. Physical and chemical analyses of the soils were performed to estimate their basic characteristics (IS: 1527(19060)) [41]. To remove organic matter, the samples were placed in an 80°C water bath and treated with 5 mL increments of 30% H_2O_2. The absence of effervescence indicated that the organic matter had been completely removed.

2.2.2. Green gram husk, black gram husk and rice husk

The crop's outer covering is known as husk, and it accounts for 20%–25% of its weight. It is typically extracted during milling and is widely used as a heating fuel in Indian households and factories. However, due to its widespread availability and low cost, it is widely used in rural India. For this investigation, the green gram husk (GGH), black gram husk (BGH) and rice husk (RH) is obtained from locally available mills. The residue, obtained after extraction with distilled water, was dried at room temperature for 48 h before ground and sieved(of 100-635 SIEVE NO ASTM E11-87). The obtained samples were stored in airtight containers for future research (to avoid entry of moisture).

2.3. Adsorption studies

Batch studies were carried out at room temperature (30°C ± 20°C) to investigate the influence of several factors (specifically, pH, adsorbent dose, beginning concentration, and contract duration). In each experiment, 100 mL of known concentration phenol solution with various concentrations of adsorbents was poured in conical flasks (250 mL) and agitated on a regular basis. The samples were equilibrated for 24 h before being extracted at the appropriate time and filtered using Whatman Filter Paper (No. 42) and phenol content was determined. Similar batch tests were carried out in order to get the kinetic data.

2.4. Soil and agro-residue blend adsorbents

In this study, a soil-agro residue blend (w/w) was applied to increase the adsorbent's adsorption ability. The

adsorption capacity has been improved by combining soil with crop residue. The existence of organic matter–clay complexes in most soils must be addressed when assessing the role of organic matter in phenol adsorption. However, with larger levels of organic matter (less than or equal to 50%), adsorption occurs primarily on organic surfaces. This is because agricultural residue (organic matter) coats the clay in the soil. This was reinforced by Stevenson [42], who cited Walker and Crawford [43], who stated that up to 10% organic matter, both mineral and organic surfaces are engaged in adsorption. Stevenson pointed out that the amount of organic matter needed to cover the clay depends on the soil type as well as the kind and amount of clay available. Various blend proportions were studied for phenol adsorption, and the best dose of the mix was determined to be 25% organic matter.

2.5. X-ray diffraction analysis

The crystalline structures of Kr, Ar, Kr-BGH, and Ar-BGH were determined using X-ray diffraction (XRD). The XRD patterns were obtained by X-ray powder diffraction.

2.6. Film-pore diffusion model and its numerical solution

If more than one step is significant in influencing the rate, an adsorption system is characterized by a set of simultaneous partial differential equations. The following factors must be considered while creating a thorough mathematical model:

(i) Rate of mass transfer in the external film;
(ii) Isotherm equations (at the solid surface it is assumed that the local liquid;
(iii) phase concentration is in equilibrium with surface concentration);
(iv) Transfer of adsorbate from the external surface to interior space. This step can be assumed to follow either one or more of the following mechanisms:
  (a) Pore diffusion [37];
  (b) Surface diffusion – (Homogeneous surface diffusion [35,37] or concentration dependent surface diffusion models [35];
  (c) Combined diffusion [37];
  (d) Branched pore diffusion model [36].

In the pore diffusion model, the aquatic solution initially spreads into pores, whereby phenol molecules are adsorbed to the inner surface of the adsorbents. In the solid diffusion model, the phenol molecules are presumed to adsorb the external surface of the adsorbents, from which they stream into the center of the particle through the solid. The combined diffusion model takes into consideration both pore diffusion and solid diffusion, while the branched model of pores takes into consideration the particle pore distribution. For the majority of these systems, analytical solutions are not possible. The implicit finite difference method of Crank–Nicolson is most commonly used to solve the set of concurrent partial differential equations that define the above models. Most recently, this type of system has been successfully used with the orthogonal collocation method. There were three different methods: implicit finite differential method of the Crank–Nicolson method, semi-analytical integration and cartesian collocations methods and Lee and McKay [44] compared the results. These models and their solutions, however, have mostly been researched for activated carbon adsorption systems. The use of these models for phenol adsorption onto unusual adsorbents has not been investigated. The adsorption of phenol onto soil-agro mixtures was studied using a film-pore diffusion model in this study.

3. Results and discussion

3.1. Soil and agro-residue blend adsorbents

In the present research work, soil-agro residue blend (w/w) was used to improve the adsorption capacity of the adsorbent. The adsorption capacity had been increased by blending soil with agro residue. The presence of organic matter – clay complexes in most of the soils needs to be considered in evaluating the importance of organic matter in phenol adsorption. However, at higher organic matter (less than or equal to 50%), adsorption will occur mostly on organic surfaces. This is due to the agro residue (organic matter) coats the clay present in the soil. This was supported by Stevenson [42] quoted Walker and Crawford [43] indicated that up to an organic matter of about 10%, both mineral and organic surfaces are involved in adsorption. Stevenson pointed out that the amount of organic matter required to coat the clay will depend on the soil type and the kind and amount of clay that is present. As studies reveal various blends proportions were studies for adsorption of phenol and the optimum dosage of the blend was found at 25% of organic matter.

3.1.1. XRD analysis for the soil and soil-agro blend samples

XRD is an effective mineral analysis tool. Kr and Kr-BGH minerals and soil-agro mixture were characterized by XRD peaks of 21.208, 26.985 and 50.509 at diffraction angles. Ar and Ar-BGH, however, were characterized by radiation peaks at 20.916, 26.780 and 50.517 at different angles and soil agro-blend minerals. Quartz (Q), iron-silicon sulfide (ISA), aluminum oxide (AO), iron silicium (IS), geothite (G) and iron oxide hydroxide are the main mineral compositions found in both soils (IOH). Iron oxides have been found in the soil fractions (such as hematite and goethite). Fe_2O_3 is common iron oxide in the form of hematite which has a characteristic peak between 33 and 36 on the scale of 2 thetas and is responsible for a red soil color. Götethite is the most common colored iron oxide in soils (with a molecular structure of FeOOH) which shows a typical peak between 20 and 22. The four sample adsorbents shown in Figs. 1 and 2 contained the minerals. Gibbsite was also a mineral, with the main peak of about 25.0° 2θ. Gibbsite is best found in the two soil samples analyzed, preferably the most common aluminum oxide in soils and in present studies. In the XRD analysis, quartz was also observed. This ore has a characteristic peak on the 2θ scale of about 22 and 27.0.

3.1.2. Adsorption kinetics

Adsorption kinetic is important for controlling process efficiency. Various kinetic models have been used by

various researchers, where the pseudo-first-order [45–47] and pseudo-second-order models were studied to investigate the adsorption process of phenol on soil (this part of work published by the author) and soil-agro residue blend system [48]. The adsorbents were separately exposed to the aqueous phenol of initial concentrations 100 mg/L and the amount of phenol adsorbed was estimated for a time period of 30–360 min.

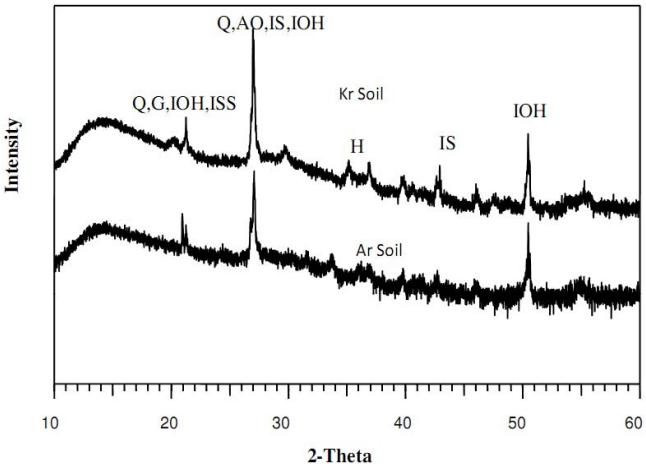

Fig. 1. XRD peaks for Kr and Ar soil.

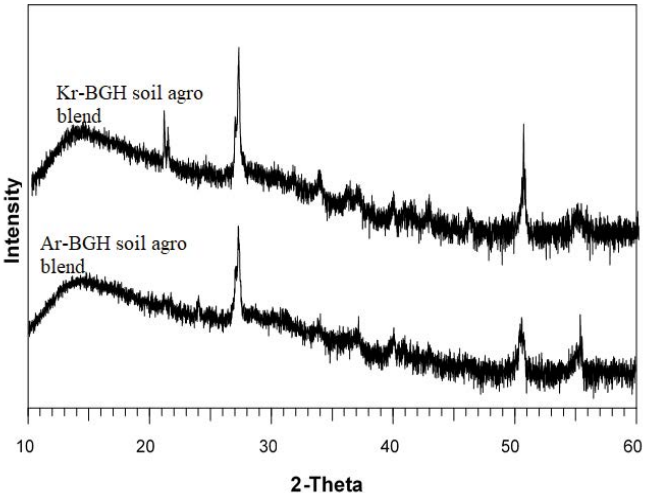

Fig. 2. XRD peaks for Kr-BGH and Ar-BGH soil-agro blend.

3.2. Diffusion kinetics

In order to determine the rate-limiting step in the adsorption process, kinetic studies of adsorption are essential. However, the overall adsorption process is assumed to occur by the following three steps:

(1) Mass transfer of a solute from the bulk solution to the particle surface (external mass transfer);
(2) Adsorption of solute onto the surface of the adsorbent.
(3) Internal mass transfer within the particle (pore diffusion or solid diffusion).

In the present research work Step (2) is assumed rapid and thus it is not considered as the rate-limiting step. Steps (1) and (3) were considered as the rate-limiting steps. In the pore diffusion model, it is assumed that the aqueous solution first diffuses into the pores wherein phenol molecules are adsorbed onto the internal surface of the adsorbents.

3.2.1. External mass transfer coefficient

In this section, the mass transport model (based on external mass transfer batch adsorption) was studied, to determining the influence of the outside boundary layer in the adsorption process. The external mass transfer coefficient for the phenol – soil and soil-agro residue blend system have been evaluated by the equation as discussed in the methodology.

3.2.2. Effect of initial phenol concentration

The initial phenol concentration of effluent is important for a given mass of adsorbent and can adsorb a certain amount of phenol, which is correlated by the equilibrium isotherm equation. The effect of initial phenol concentration was studied. The $\ln(C_t/C_0)$ against time plots are shown in Figs. 3–8 for the adsorption of phenol on soils (Kr and Ar) as well as soil-agro residue (Kr-BGH, Ar-BGH, Kr-GGH, Kr-RH). The fractional adsorption was low at high concentrations, while the initial absorption of phenol was quick at low concentrations, indicating quick surface adsorption

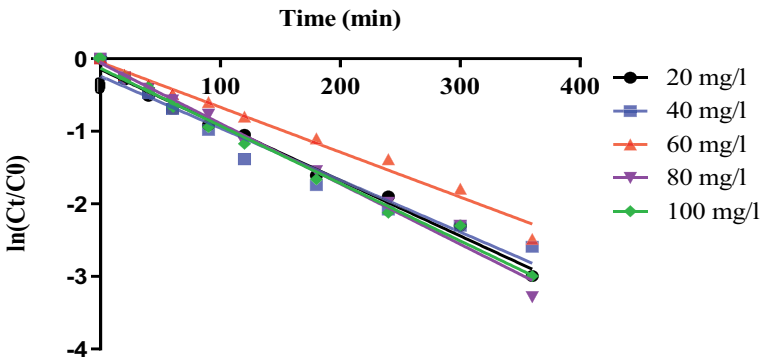

Fig. 3. $\ln(C_t/C_0)$ against time plot with different initial concentration systems (Kr soil).

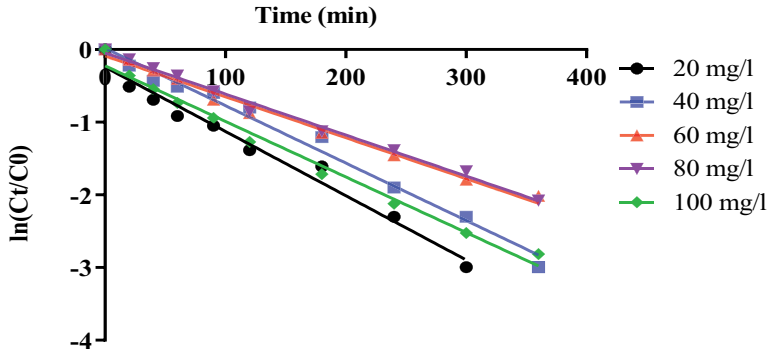

Fig. 4. $\ln(C_t/C_0)$ against time plot with different initial concentration systems (Ar soil).

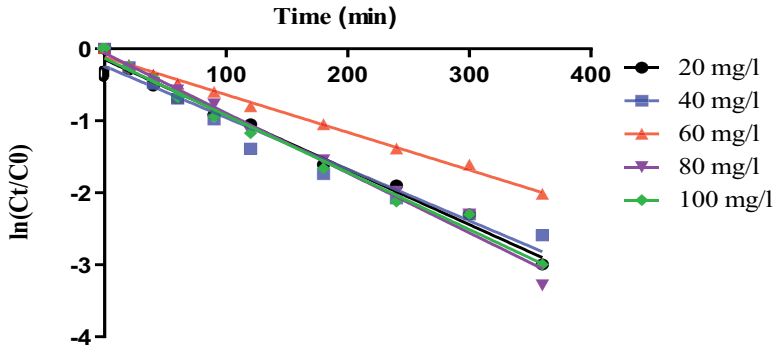

Fig. 5. $\ln(C_t/C_0)$ against time plot with different initial concentration systems (Kr-BGH soil blend).

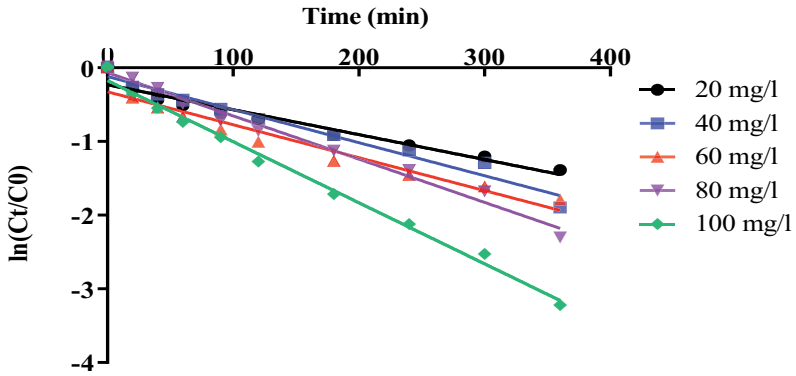

Fig. 6. $\ln(C_t/C_0)$ against time plot with different initial concentration systems (Ar-BGH soil blend).

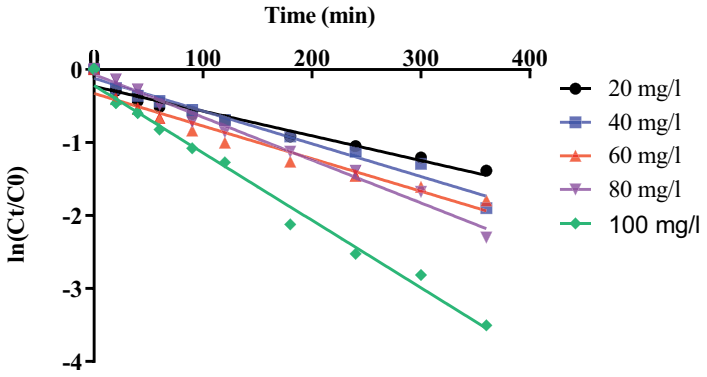

Fig. 7. $\ln(C_t/C_0)$ against time plot for phenol with different initial concentration systems (Kr-RH soil blend).

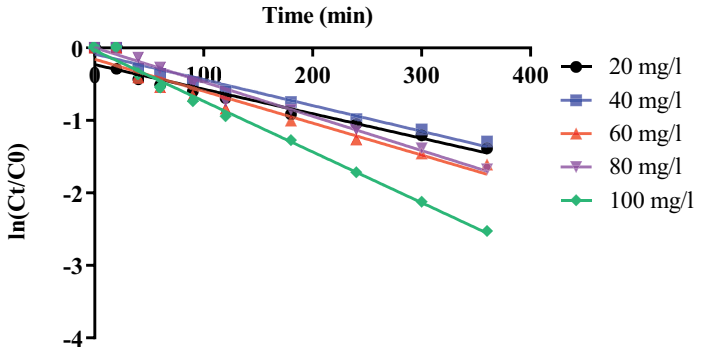

Fig. 8. $\ln(C_t/C_0)$ against time plot with different initial concentration systems (Kr-GGH soil blend).

Table 2
External mass transfer coefficient for phenol system with different initial concentrations (soil and soil-agro residue blend)

Concentration	Kr soil	Ar soil	Kr-BGH	Ar-BGH	Kr-GGH	Ar-GGH	BGH-RH
(mg/L)	K_f (cm/s)	K_f (cm/s)	K_f (cm/s)	K_f (cm/s)	K_f (cm/s)	K_f (cm/s)	K_f (cm/s)
20	2.45×10^{-5}	1.28×10^{-5}	9.37×10^{-5}	3.15×10^{-5}	2.22×10^{-5}	1.54×10^{-5}	1.08×10^{-5}
40	2.02×10^{-5}	1.15×10^{-5}	8.77×10^{-5}	4.18×10^{-5}	2.95×10^{-5}	1.62×10^{-5}	1.16×10^{-5}
60	1.75×10^{-5}	8.17×10^{-6}	6.41×10^{-5}	4.17×10^{-5}	2.94×10^{-5}	2.01×10^{-5}	1.43×10^{-5}
80	1.25×10^{-5}	8.17×10^{-6}	1.02×10^{-4}	5.47×10^{-5}	3.86×10^{-5}	2.16×10^{-5}	1.87×10^{-5}
100	6.31×10^{-6}	8.17×10^{-6}	9.72×10^{-5}	7.72×10^{-5}	6.07×10^{-5}	3.19×10^{-5}	2.36×10^{-5}

in the case of two natural soils as well as soil-agro residue blends. As a result, the amount of phenol in the effluent affects the extent and rate of phenol absorption on two native soils as well as soil-agro residue blends. As a result, the amount of phenol in the effluent affects the extent and rate of phenol absorption on two native soils as well as soil-agro residue blends. The external mass transfer coefficients, 'K_f,' were calculated using equation '04'. Table 2 shows the external mass coefficients, 'K_f,' at varied beginning concentrations. The driving force for mass transfer is determined by the concentration gradient across the film and the accessible external adsorbent surface area. However, the driving force for mass transfer is dependent and is based on the differential between the bulk liquid concentration and the particle surface liquid concentration. As a result, the external mass transfer coefficients appear to grow as initial C_0 increases.

3.2.3. Effect of adsorbent mass

The effect of adsorbent mass was studied on the phenol when the other experimental conditions were maintained constant. In this case, C_0 is constant, the mass of the adsorbent is increased, increases its surface and thus the rate of the phenol removal is increased. Table 2 shows the values of K_f. There is limited data available for external mass transfer coefficients reported in the literature, using activated carbon, as 2×10^{-3} cm/s and 1×10^{-3} cm/s for AB25 and BY11 respectively [49]. Keith et al. [50] reported, K_f, as 3.11×10^{-4} cm/s and 3.85×10^{-4} cm/s for the adsorption of AB80 and AY117 onto carbon, respectively. For phenol, the order of external mass transfer coefficients K_f was reported as 10^{-4} cm/s. The values of the external mass transfer coefficients obtained in this work varying in the range of 1.04×10^{-6} cm/s to 1.76×10^{-4} cm/s. Moreover, the mean values of K_f for Kr soil were 3.75×10^{-5} cm/s, for Ar soil 2.04×10^{-5} cm/s for Kr-BGH 2.12×10^{-5} cm/s and for Ar-BGH 1.486×10^{-4} cm/s are very close to the K_f reported in the literature [49]. Since the particle size is constant, the surface area will be directly proportional to the mass of the adsorbent system. The K_f values in Table 2 are dependence on mass of the adsorbent. In fact, K_f decreases with increasing the mass of adsorbent. This effect is probably due to the fact that for bigger masses a small amount of external surface is presented to the adsorption of phenol and therefore there is a large driving force per unit surface area of adsorbent. When the external mass coefficients of each individual adsorbent employed in this study are compared, Ar-BGH and Kr-RH adsorbents exhibit less resistance than Kr soil, Ar soil, and Kr-BGH adsorbents. This is because organic matter (owing to the presence of cellulose and lignin) covers the soil sample, requiring higher driving power per unit surface area. The external mass transfer model is influenced by the thickness of the boundary layer as well as relevant physical properties such as liquid viscosity, particle diameter, particle density and temperature. The apparent changes in K_f with initial phenol concentration and mass are probably may be due to the two-resistance mechanism (i.e., external mass transfer and internal mass transfer). The external mass transfer may have very little effect on the rate control process which may be predominated by the intraparticle diffusion. This model will be tested in section 3.3.

3.3. Intraparticle diffusion model

In this section the mass transport model is based on intraparticle diffusion is the only rate-controlling step for

adsorption. The experiment contact time results can be used to establish the time dependence of the system. The intraparticle diffusion rate parameters for the sorbate-sorbent system have been evaluated by the equation:

$$q_t = K \times t^{0.5} \tag{14}$$

The intraparticle diffusion K can be calculated from the initial slope of q_t vs. $t^{0.5}$.

3.3.1. Effect of initial phenol concentration

Figs. 9–14 depict the plots of phenol uptake, 'q_t', against the square root of time '$t^{0.5}$' for various initial phenol concentrations. Intraparticle diffusion is responsible for the linear portion of the plots. Using the '$t^{0.5}$' plots, all previous studies for the adsorption surfactants on activated carbon [51], Victoria Blue and Basic Blue 26 dye carbon, different types of dyes onto agriculture by-products, phenol, cresols and nitro-phenols on fly-ash and basic dyes on water hyacinth confirms the phenomenon of intraparticle diffusion. Previous studies confirmed that plots between 'q_t' vs. '$t^{0.5}$' result in a single gradient line (Figs. 9–14). In several cases, the linearized plot does not go through the origin, that is, $q_t = 0$, $t^{0.5} = 0$, which has been attributed to an initial boundary layer resistance that is the rate-controlling for the first 10% of the adsorption capacity [52–55]. Figs. 9–14 show that each plot can be represented reasonably well by a single straight line. There is some deviation at the origin, which could be due to external mass transfer resistance.

Table 3 shows the values of 'K' for phenol adsorption onto two natural soils and a soil-agro blend as a function of initial phenol concentration. The intraparticle rate parameters for intraparticle diffusion have been evaluated.

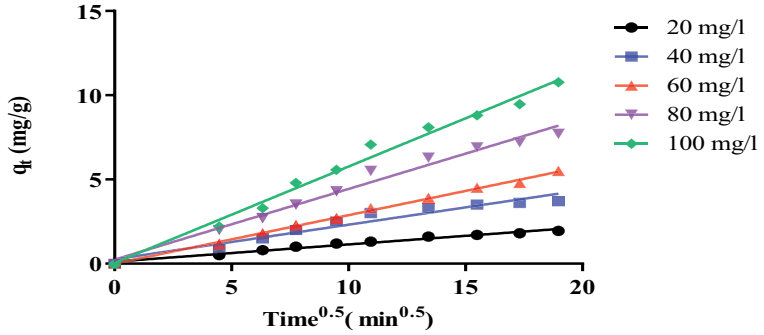

Fig. 9. 'q_t' against '$t^{0.5}$' plot for phenol with different initial concentration systems (Kr soil).

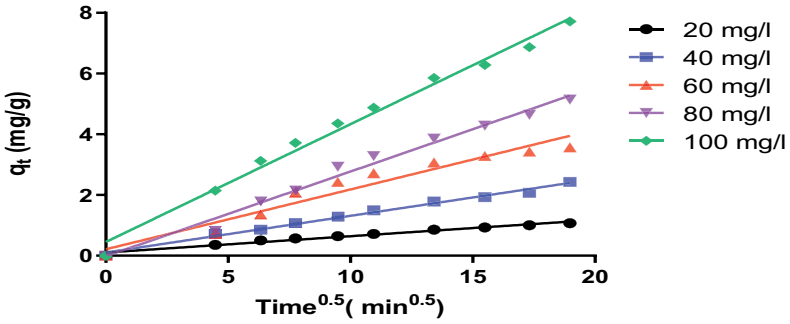

Fig. 10. 'q_t' against '$t^{0.5}$' plot for phenol with different initial concentration systems (Ar soil).

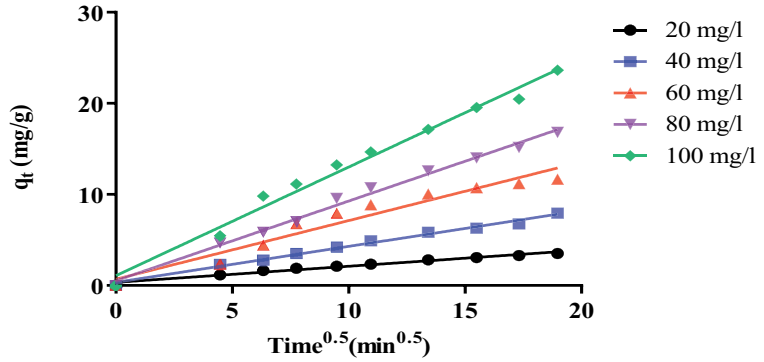

Fig. 11. 'q_t' against '$t^{0.5}$' plot with different initial concentration systems (Kr-BGH).

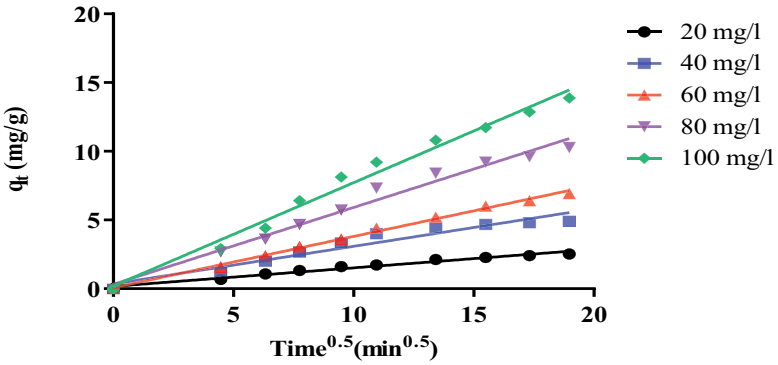

Fig. 12. 'q_t' against '$t^{0.5}$' plot with different initial concentration systems (Ar-BGH soil).

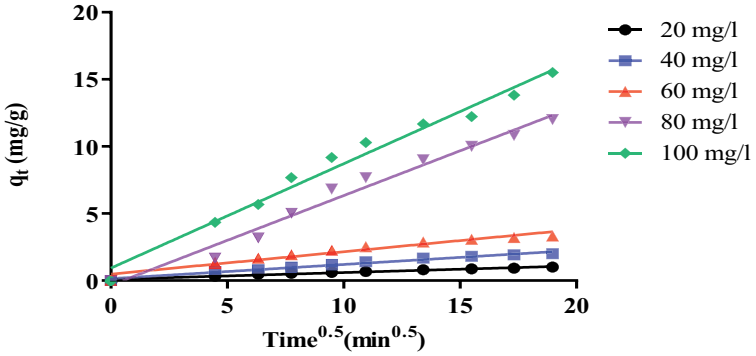

Fig. 13. 'q_t' against '$t^{0.5}$' plot with different initial concentration systems (BGH-RH).

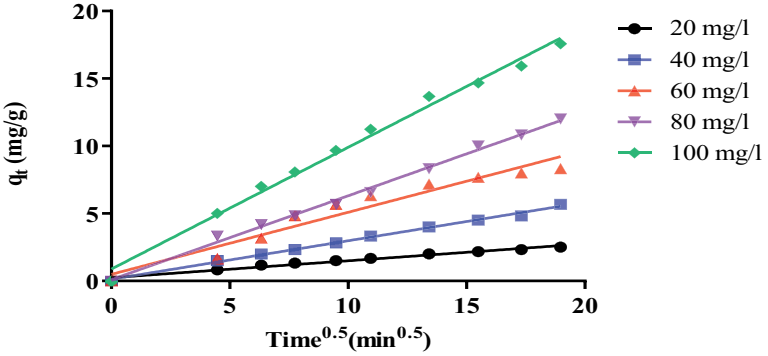

Fig. 14. 'q_t' against '$t^{0.5}$' plot with different initial concentration systems (Kr-GGH).

Table 3
Intraparticle rate parameters of phenol system with different initial concentration (soil and soil-agro residue blend)

C_0 (mg/L)	Kr soil (mmol phenol/gmin$^{0.5}$)	Ar soil (mmol phenol/gmin$^{0.5}$)	Ar BGH (mmol phenol/gmin$^{0.5}$)	Kr GGH (mmol phenol/gmin$^{0.5}$)	Kr BGH (mmol phenol/gmin$^{0.5}$)	Kr RH (mmol phenol/gmin$^{0.5}$)
	K (× 10^{-3})	K (× 10^{-3})	K (× 10^{-3})	K (× 10^{-3})	K (× 10^{-3})	K (× 10^{-3})
20	1.17	0.603	1.510	1.410	1.980	0.562
40	2.37	1.328	3.160	3.100	4.340	1.180
60	3.11	2.255	4.050	4.800	7.440	1.920
80	4.55	3.124	6.240	7.470	9.580	7.470
100	6.32	4.313	8.250	9.048	12.100	8.680

The use of this model for design applications is limited due to a large number of '*K*' values unless the rate parameters can be correlated against system parameters. Fig. 15 depicts a plot of 'ln*K*' vs. 'lnC_0' for phenol adsorption onto two natural soils and a soil-agro blend. Eq. (15) depicts the line's equation. This equation has a generic form, which is as follows:

$$K = AC_0^B \tag{15}$$

Table 4 displays the values of *A* and *B* for the phenol adsorption onto two natural soils and soil-agro blends. As shown in Fig. 15, there is a gradual increase in '*K*' with an increase in C_0, indicating that increasing the bulk liquid concentration increases the driving force of phenol from the bulk into the solid particle. The linearity of the '$t^{0.5}$' plots indicates that intraparticle diffusion is the main rate-controlling step throughout most of the adsorption process.

3.3.2. Numerical solution of the non-linear adsorption system

The bulk concentration-time curve for batch adsorption using pore-diffusion was predicted using the effect of phenol concentration based on external mass transfer and intraparticle diffusion. The internal diffusion coefficients were calculated using the numerical solution. The external mass transfer coefficient 'K_f' and the solid phase diffusion coefficient 'D_e' were the primary parameters required for program use. Using the best-fit isotherm equation, it is possible to obtain the average best fit for each phenol-soil and soil-agro blend system by minimizing the difference between the theoretical and experimental decay curves for batch adsorption (in this case, the Langmuir isotherm). Figs. 16–20 show the experimental concentration decay data along with the predicted decay curves, where there is

Table 4
Values of the correlative constants, *A* and *B*, in the intraparticle rate equation for the effect of initial phenol concentration

Adsorbent system	Intraparticle diffusion		
	A	*B*	R^2
Kr soil	5.52×10^{-5}	1.012	0.9877
Ar soil	1.54×10^{-5}	1.217	0.9988
Kr-BGH	6.89×10^{-5}	1.026	0.9874
Ar-BGH	4.15×10^{-5}	1.169	0.9973
Kr-GGH	6.67×10^{-5}	1.1694	0.9974
Ar-GGH	2.150×10^{-5}	1.777	0.918

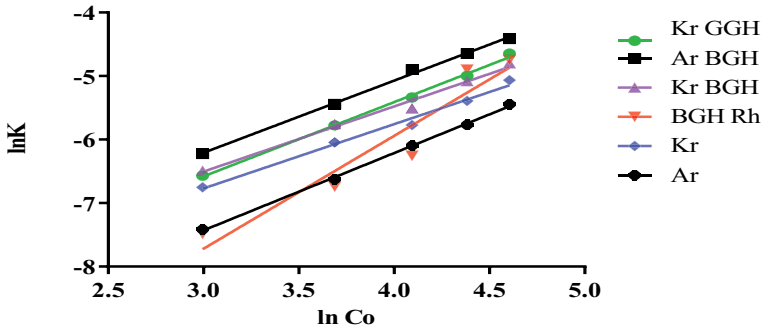

Fig. 15. 'ln(*K*)' against 'ln(C_0)' plot for different sorbate-sorbent system.

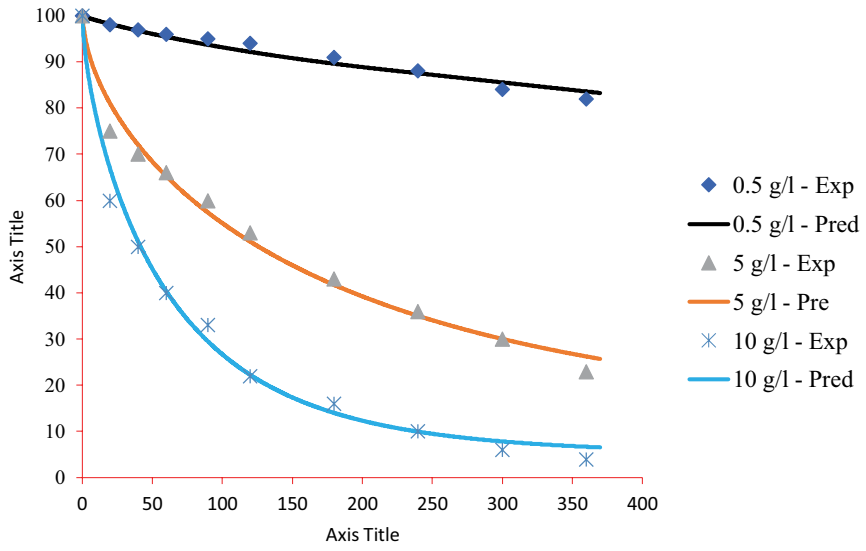

Fig. 16. Effect of intial adsorbent on the adsorption of phenol onto Kr soil.

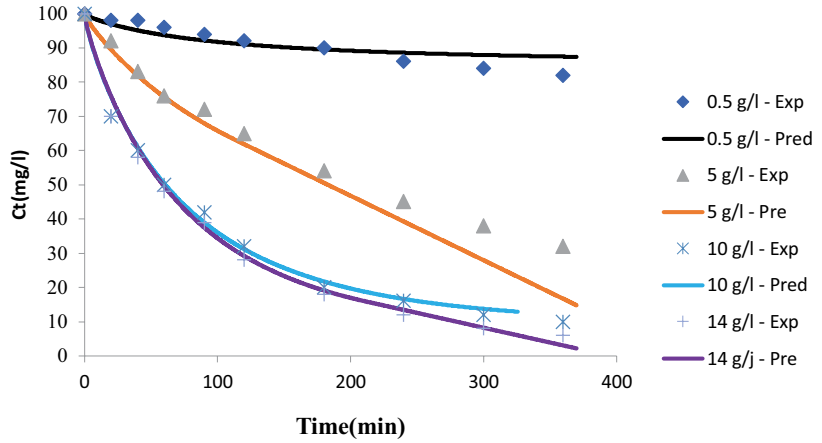

Fig. 17. Effect of intial adsorbent on the adsorption of phenol onto Ar soil.

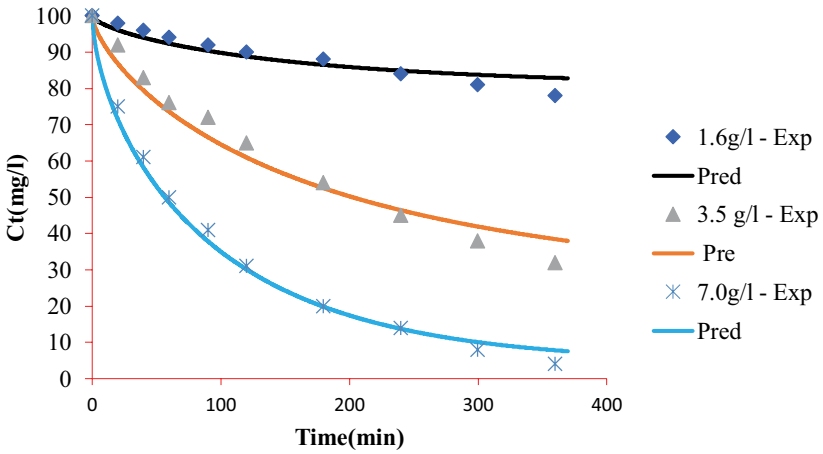

Fig. 18. Effect of intial adsorbent on the adsorption of phenol onto Kr-BGH.

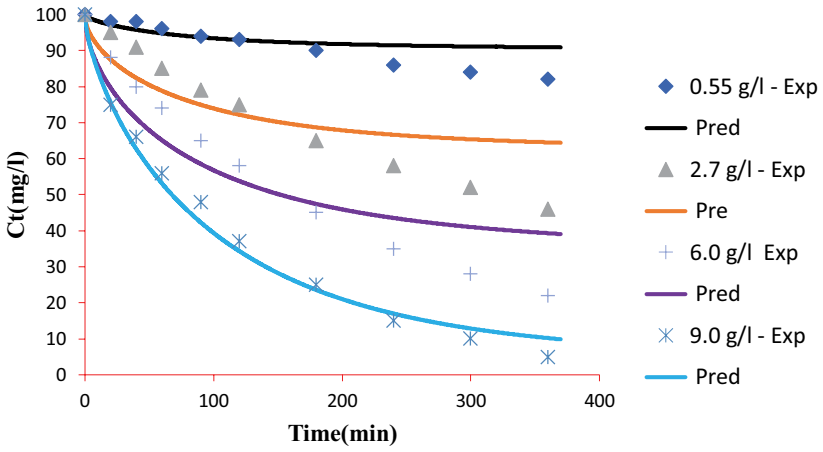

Fig. 19. Effect of intial adsorbent on the adsorption of phenol onto Ar-BGH blend.

a good correlation between the experimental data and theoretical results. However, at a low adsorbent, the correlation was to be comparatively poor (as described in section 4.8.2). Tables 2 and 5 show the values of the external mass transfer coefficients obtained in this work.

3.4. Infrared characterization of individual adsorbents

3.4.1. Infrared characterization of soil-agro blend residue

Figs. 21 and 22 show the Fourier-transform infrared spectroscopy (FTIR) spectra of soil-agro residue blend

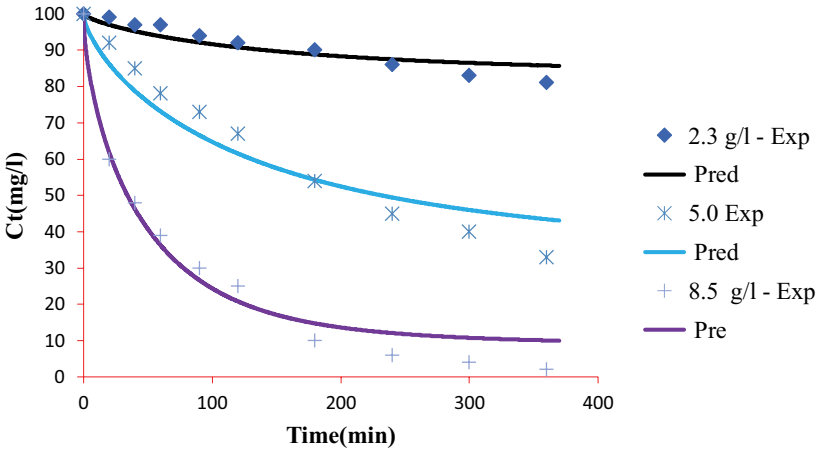

Fig. 20. Effect of intial adsorbent on the adsorption of phenol onto Kr-GGH blend.

Table 5
External mass transfer coefficient for phenol system with different masses (soil and soil-agro residue blend)

Kr soil	Ar soil	Ar-BGH	Ar-GGH	Kr-GGH	Kr-BGH	BGH-RH
K_f (cm/s)	K_f (cm/s)	K_f (cm/s)	K_f (cm/s)	K_f (cm/s)	K_f (cm/s)	K_f (cm/s)
3.167×10^{-5}	3.15×10^{-5}	1.33×10^{-4}	1.28×10^{-4}	1.42×10^{-4}	6.37×10^{-5}	7.33×10^{-5}
2.0×10^{-5}	1.75×10^{-5}	1.76×10^{-4}	1.27×10^{-4}	1.56×10^{-4}	6.16×10^{-5}	6.50×10^{-5}
2.33×10^{-5}	1.64×10^{-5}	1.37×10^{-4}	1.23×10^{-4}	1.56×10^{-4}	1.56×10^{-4}	5.67×10^{-5}
–	1.63×10^{-5}	–	8.25×10^{-6}	1.04×10^{-4}	–	3.67×10^{-5}

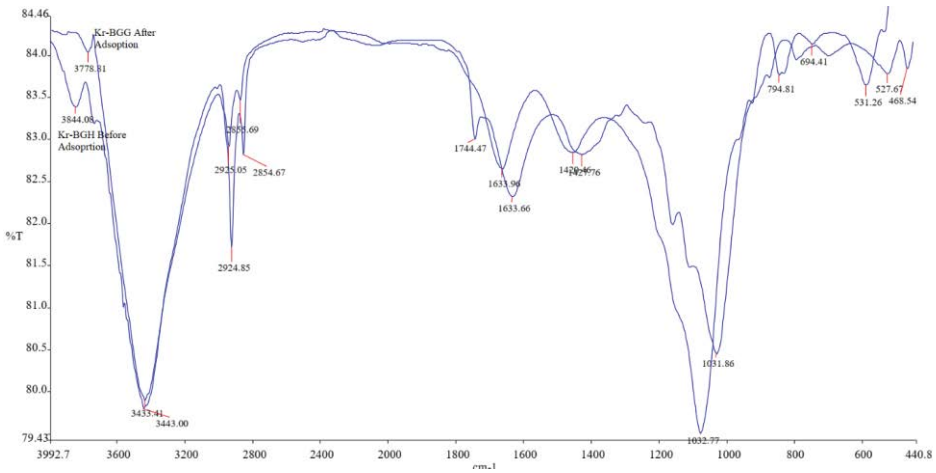

Fig. 21. FTIR analysis of Kr-BGH blend before and after adsorption.

namely Kr-BGH and Ar-BGH, as well as the percentage transmission for various wavenumbers, absorption bands identified in the spectra and their assignment to the corresponding functional group. The OH stretching is assigned to the characterization bands of the Kr-BGH agro residue blend that appear at 3,844.08 and 3,433.00 cm^{-1} as bands. The peaks of 2,924.85 and 2,854.67 cm^{-1} as bands are assigned to C–H methyl and methylene stretching. At 1,744.47 cm^{-1} one small trough was observed, that stretch indicates the C=O carbonyls group. A peak at 1,633.66 cm^{-1} was observed, indicating stretching vibration of C–O bonds caused by non-ionic carboxyl groups (–COOH, $–COOCH_3$) and may be assigned to hydrogen bonding between carboxylic acids or their esters [54] and ammonium ions. The band at 1,427.76 cm^{-1} corresponds to the symmetric bending of CH_3 stretching. The wavelength range of 1,375 to 1,000 cm^{-1} is assigned to various stretches indicating C–O stretching of COOH, $–SO_3$ is stretching, O–H alcohols and aliphatic ethers and C–O stretching of COOH. A peak at 1,031.86 cm^{-1} was observed and may be possible for all or a

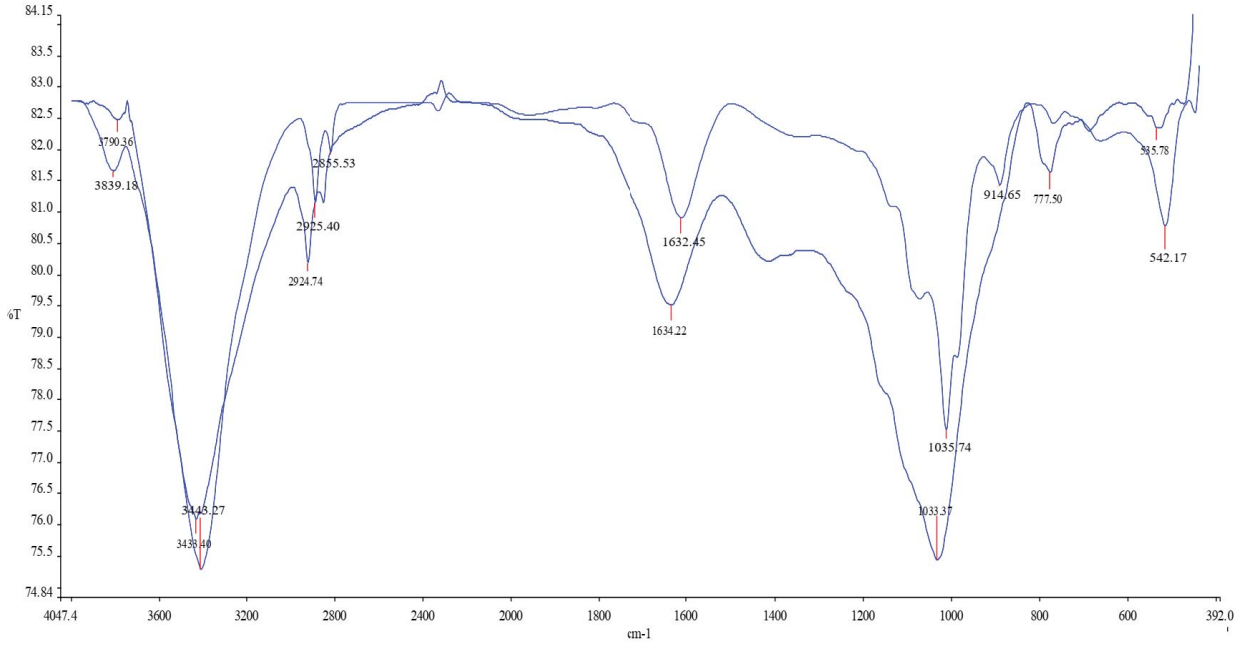

Fig. 22. FTIR analysis of Ar-BGH blend before and after adsorption.

few stretches. The band at 527.67 cm^{-1} can be attributed to typical O–Si–O bending vibration and also assigned C–H bending at a wavelength range of 990–690 cm^{-1}. The absorption bands of a bonded hydroxyl group (OH) can be seen in the Ar-BGH spectrum the 3,790.36 and at 3,433.40 cm^{-1}. The C–H methyl and methylene groups are represented by the band at 2,924.74 cm^{-1} stretching. Because the OH stretching band at 3,433.40 cm^{-1} indicates the presence of some interlamellar water, the band at 1,634.22 cm^{-1} corresponds to the OH deformation of water [56]. The carboxylic group is represented by 1,634.22 cm^{-1} stretching in the same band. The trough at 1,033.37 cm^{-1} is assigned to the asymmetric stretching vibration of Si–O–Si of soil, as well as different stretches indicating C–O stretching of COOH, $–SO_3$ stretching, O–H alcohols and aliphatic ethers, and C–O stretching of COOH at the wavelength range of 1,375–1,000 cm^{-1}. The majority of the quartz stretching properties produce a small trough at 777.50 cm^{-1}. The stretching vibration of C–H bending is assigned to the trough at 535.78 cm^{-1}. According to various studies [57], agro-residues mostly consist of cellulose, hemicelluloses, lignin, pectin, and extractive (fat, waxes, etc.) ions that are generally sorbed to carboxylic ions (mainly present in hemicelluloses, pectin, lignin). This might explain the presence of complicated functional groups in the FTIR data.

3.4.2. Effect of phenol-sorption on functional groups of the adsorbents

Adsorption/adsorption interactions with carbon have led to certain spectral changes, such as the demise of several bands, an expansion of certain bands and spectral shifts. Spectral variations in the spectra of the unloaded and loaded adsorbents are on the basis of the changes in the nature of the surface. Comparing fresh adsorbents FTIR with adsorbing phenol FTIR, a shift in wavenumbers of dominant phenol peaks has been observed. This shift in the wavelength is shown in Figs. 21 and 22 showing that phenol binding was performed on the adsorbent surface. The wavenumber from the different groups were observed and new peaks on the adsorbed phenol were observed. Compare Figs. 21 and 22, there is no shift in the range of 1,350–1,000 cm^{-1} (O–H alcohols and aliphatic ethers), and no shift in the region of 1,300–1,000 cm^{-1} (C–O stretching of COOH). O–H stretching was observed to shift in wavenumber in the case of Kr soil and Ar soil, respectively.

Similarly, there were few new peaks in the 913.69, 874.54, 694.71 and 473.46 cm^{-1} wavenumbers were observed in the Kr soil. A shift was observed at wave number from 533.07 to 530.49 cm^{-1} (C–X stretching). Figs. 21 and 22, respectively, show the FTIR spectrum of Kr-BGH soil agro-residue combinations before and following adsorption. A shift was observed at a peak of 3,443.00 to 3,433.41 cm^{-1} indicating stretching of the N–H primary amine group. At a wavenumber of 1,427.76 cm^{-1}, a shift was observed as 1,420.46 cm^{-1}, indicating symmetric bending of CH_3. A new peak with 794.81 cm^{-1} was observed, indicating the aromatic C–H stretching group and also showing the highest quartz detection features. At 527.67 to 531.26 cm^{-1} a shift was found, indicating the degree of C–X group expansion.

4. Conclusion

An external mass transfer, pore and surface diffusion model have been studied in this study. The results indicate that both pore and surface diffusion are primarily responsible for the adsorption process. The effective diffusion coefficient and the solid phase equilibrium concentration vary over time. For each data set, an analytical solution can be provided for effective diffusivity. Research indicates that

both pore and surface diffusion are involved in the mechanism of mass transfer of soil-agro-based phenol. The film-pore-surface diffusion model provides a major improvement. A good correlation between the experimental data and theoretical results was evident for high adsorbent mass than lower. The rate-limiting step of phenol adsorption onto soil-ago blends were a combination of a chemical reaction and diffusion adsorption, diffusion adsorption plays a significant role in the rate-determining step.

Acknowledgment

The author would like to thank Dr. Ashutosh Das, PRIST Deemed to be University, Thanjavur, India.

References

[1] Agency for Toxic Substances and Disease Registry (ATSDR), Toxicological Profile for Phenol Atlanta, U.S. Department of Health and Human Services, GA, 1998.
[2] M. Abhijit, D.G. Sunando, K.B. Jayant, D. Sirshendu, Adsorption of arsenite using natural laterite as adsorbent, Sep. Purif. Technol., 55 (2007) 350–359.
[3] N. Ahalya, R.D. Kanamadi, T.V. Ramachandra, Biosorption of chromium(VI) from aqueous solutions by the husk of Bengal gram (*Cicer arientinum*), Electron. J. Biotechnol., 8 (2005) 258–264.
[4] C. Aharoni, F.C. Tompkins, Kinetics of Adsorption and Desorption and the Elovich Equation, D.D. Eley, H. Pines, P.B. Weisz, Eds., Advances in Catalysis and Related Subjects, Academic Press, New York, 1970, pp. 1–49.
[5] C. Aharoni, D.L. Sparks, S. Levinson, I. Ravina, Kinetics of soil chemical reactions: relationships between empirical equations and diffusion models, Soil Sci. Soc. Am. J., 55 (1991) 1307–1312.
[6] M. Ahmedna, W.E. Marshall, A.A. Husseiny, I. Goktepe, R.M. Rao, The use of nutshell carbons in drinking water filters for removal of chlorination by-products, J. Chem. Technol. Biotechnol., 79 (2004) 1092–1097.
[7] J.M. Akhtar, M.H. Syed, M.I. Bhanger, S. Iqbal, Low-cost sorbents for the removal of methyl parathion pesticide from aqueous solutions, Chemosphere, 66 (2007) 1829–1838.
[8] I. Akira, K. Nobuyuki, Y. Jin, O. Ken-Ichi, Liquid phase adsorption equilibrium of phenol and its derivatives on macroreticular adsorbents, J. Chem. Eng. Jpn., 17 (1984) 389–395.
[9] S.A. Boyd, M.M. Mortland, C.T. Chiou, Sorption characteristics of organic compounds on hexadecyltrimethylammonium-smectite, Soil Sci. Soc. Am. J., 52 (1988) 652–657.
[10] F.B. Maria, C. Fulvio, G.F. Carlo, M. Silvia, M. Luca, P. Luciano, Interaction between montmorillonite and pollutants from industrial wastewaters: exchange of Zn^{2+} and Pb^{2+} from aqueous solutions, Appl. Clay Sci., 9 (1995) 383–395.
[11] M. Gutierrez, H.R. Fuentes, A mechanistic modeling of montmorillonite contamination by cesium sorption, Appl. Clay Sci., 11 (1996) 11–24.
[12] B. Lo, R. Mak, S. Lee, Modified clays for waste containment and pollutant attenuation, J. Environ. Eng. (New York), 123 (1997) 25–32.
[13] F.A. Banat, B. Al-Bashir, S. Al-Asheh, O. Hayajneh, Adsorption of phenol by bentonite, Environ. Pollut., 107 (2000) 391–398.
[14] O. Hassan, D. Younes, M. Hamou, M. Lahcen, A. Mohamed, Kinetic, isotherm and mechanism investigations of the removal of phenols from water by raw and calcined clays, Heliyon, 5 (2019) e01616, doi: 10.1016/j.heliyon.2019.e01616.
[15] G. Sheng, S.A. Boyd, S. Xu, A dual function organoclay sorbent for lead and chlorobenzene, Soil Sci. Soc. Am. J., 63 (1999) 73–78.
[16] L. Ma, Q. Chen, J. Zhu, Y. Xi, H. He, R. Zhu, Q. Tao, G.A. Ayoko, Adsorption of phenol and Cu(II) onto cationic and zwitterionic surfactant modified montmorillonite in single and binary systems, Chem. Eng. J., 283 (2016) 880–888.
[17] T. Lehlogonolo, T. Shepherd, L. Frederick, C. Evans, Adsorption of phenol from wastewater using calcined magnesium-zinc-aluminium layered double hydroxide clay, Sustainability, 12 (2020) 4273, doi: 10.3390/su12104273.
[18] L.S. Tabana, R.P. Ledikwa, S.M. Tichapondwa, Adsorption of phenol from wastewater using modified layered double hydroxide clay, Chem. Eng. Trans., 76 (2019) 1267–1272.
[19] D. Kaliannan, S. Palanimanikkam, V. Palanivel, M.A. Mahadeo, B.N. Ravindra, J. Shim, A novel approach to preparation of nano-adsorbent from agricultural wastes (*Saccharum officinarum leaves*) and its environmental application, Environ. Sci. Pollut. Res., 26 (2019) 5305–5314.
[20] H.D. Bouras, O. Benturki, N. Bouras, M. Attou, A. Donnot, A. Merlin, F. Addoun, M.D. Holtz, The use of an agricultural waste material from *Ziziphus jujuba* as a novel adsorbent for humic acid removal from aqueous solutions, J. Mol. Liq., 211 (2015) 1039–1046.
[21] Y.F. Lam, L.Y. Lee, S.J. Chua, S.S. Lim, S. Gan, Insights into the equilibrium, kinetic and thermodynamics of nickel removal by environmental friendly *Lansium domesticum* peel biosorbent, Ecotoxicol. Environ. Saf., 127 (2016) 61–70.
[22] K. Johari, N. Saman, S.T. Song, C.S.H. Kong, H. Mat, Adsorption enhancement of elemental mercury by various surface modified coconut husk as ecofriendly low-cost adsorbents, Int. Biodeterior. Biodegrad., 109 (2016) 45–52.
[23] G.F. Malash, M.I. El-Khaiary, Piecewise linear regression: a statistical method for the analysis of experimental adsorption data by the intraparticle-diffusion models, Chem. Eng. J., 163 (2010) 256–263.
[24] C. Yao, T. Chen, A new simplified method for estimating film mass transfer and surface diffusion coefficients from batch adsorption kinetic data, Chem. Eng. J., 265 (2015) 93–99.
[25] K.M. Thomas, W.J. Weber, A predictive model for the design of fluid-bed adsorbers, J. Water Pollut. Control Fed., 40 (1968) 741–765.
[26] R.H. Mohammed, O. Mesalhy, M.L. Elsayed, L.C. Chow, Scaling analysis of heat and mass transfer processes in an adsorption packed bed, Int. J. Therm. Sci., 133 (2018) 82–89.
[27] P. Agnes, E.B. Naidoo, A.E. Ofomaja, Intraparticle diffusion of Cr(VI) through biomass and magnetite coated biomass: a comparative kinetic and diffusion study, S. Afr. J. Chem. Eng., 32 (2020) 39–55.
[28] L.M.S. Silva, M.J. Muñoz-Peña, J.R. Domínguez-Vargas, T. González, E.M. Cuerda-Correa, Kinetic and equilibrium adsorption parameters estimation based on a heterogeneous intraparticle diffusion model, Surf. Interfaces, 22 (2021) 100791, doi: 10.1016/j.surfin.2020.100791.
[29] A. Pholosi, E.B. Naidoo, A.E. Ofomaja, Clean application of magnetic biomaterial for the removal of As(III) from water, Environ. Sci. Pollut. Res., 25 (2018) 30348–30365.
[30] A. Pholosi, E.B. Naidoo, A.E. Ofomaja, Batch and continuous flow studies of Cr(VI) adsorption from synthetic and real wastewater by magnetic pinecone composite, Chem. Eng. Res. Des., 153 (2020) 806–818.
[31] D.D. Do, Adsorption Analysis: Equilibria and Kinetics, Imperial College Press, London, 1998.
[32] X.J. Hu, Multi-component adsorption equilibrium of gases in zeolites: effect of pore size distribution, Chem. Eng. Commun., 174 (1999) 201–214.
[33] X.J. Hu, S. Qiao, D.D. Do, Multi-component adsorption kinetics of gases in activated carbon: effect of pore size distribution, Langmuir, 15 (1999) 6428–6437.
[34] A.P. Mathews, W.J. Weber, Effect of external mass transfer and intraparticle diffusion on adsorption rates in slurry reactors, ACS Symp. Ser., 73 (1977) 91–94.
[35] W.J. Weber, J.C. Morris, Preliminary appraisal of advanced waste treatment processes, Process Int. Conf. Adv. Water Resour., 2 (1962) 231–241.
[36] J. Crank, The Mathematics of Diffusion, Oxford Clarendon Press, London, 1977.
[37] G. McKay, S.J. Allen, I.F. McConvey, M.S. Otterburn, Transport processes in the sorption of colored ions by peat particles, J. Colloid Interface Sci., 80 (1981) 323–339.

[38] G.E. Boyd, A.W. Adamson, L.S. Myers, The exchange adsorption of ions from aqueous solutions by organic zeolites. II. Kinetics, J. Am. Chem. Soc., 69 (1947) 2836–2848.
[39] J. Crank, The Mathematics of Diffusion, 2nd ed., Oxford University Press, London, 1975, pp. 69–88.
[40] V.C. Srivastava, M.M. Swamy, I.D. Mall, B. Prasad, I.M. Mishra, Adsorptive removal of phenol by bagasse fly ash and activated carbon: equilibrium, kinetics and thermodynamics, Colloids Surf., A, 272 (2006) 89–104.
[41] V.K.C. Lee, G. McKay, Comparison of solutions for the homogeneous surface diffusion model applied to adsorption systems, Chem. Eng. J., 98 (2004) 255–264.
[42] F.J. Stevenson, In: D.D. Kaufman, G.G. Still, G.D. Paulson, S.K. Bandal, Y.H. Su, H.C. Lin, Eds., Bound and Conjugated Pesticide Residues, ACS Symposium Series, 1976, pp. 180–207.
[43] Indian Standard Methods of Chemical Analysis of Fireclay and Refractory Materials IS: 1527, 1960.
[44] A. Walker, D.V. Crawford, The Role of Organic Matter in Adsorption of the Triazine Herbicides by Soils, In: Isotopes und Radiation in Orgmic Mutter Studies, International Atomic Energy Agency, Vienna, 1968, pp. 91–105.
[45] Y.S. Ho, G. McKay, Pseudo-second-order model for sorption processes, Process Biochem., 34 (1999) 451–465.
[46] Y.S. Ho, J.C.Y. Ng, G. McKay, Kinetics of pollutant sorption by bio-sorbents: review, Sep. Purif. Methods, 29 (2000) 189–232.
[47] B. Subramanyam, A. Das, Linearized and non-linearized isotherm models comparative study on adsorption of aqueous phenol solution in soil, Int. J. Environ. Sci. Technol. (Tehran), 6 (2009) 633–640.
[48] B. Subramanyam, Liquid-phase adsorption of phenol onto blended adsorbents through bioremediation, Desal. Water Treat., 92 (2017) 181–195.
[49] G. McKay, S.J. Allen, Pore diffusion model for dye adsorption onto peat in batch adsorbents, Can. J. Chem. Eng., 62 (1984) 340–345.
[50] K.H. Keith, Choy, F.P. John, G. McKay, Film–pore diffusion models—analytical and numerical solutions, Chem. Eng. Sci., 59 (2004) 501–512.
[51] F.-C. Wu, R.-L. Tseng, R.-S. Juang, Initial behavior of intraparticle diffusion model used in the description of adsorption kinetics, Chem. Eng. J., 53 (2009) 1–8.
[52] G. McKay, Basic dye adsorption on activated carbon, Water Air Soil Pollut., 12 (1978) 307–317.
[53] S.S. Nawar, H.S. Doma, Removal of dyes from effluents using low-cost agricultural by-products, Sci. Total Environ., 79 (1989) 271–279.
[54] B.K. Singh, N.S. Rawat, Comparative sorption kinetic studies of phenolic compounds on fly ash and impregnated fly ash, J. Chem. Technol. Biotechnol., 61 (1994) 57–65.
[55] K.S. Low, C.K. Lee, K.K. Tan, Biosorption of basic dyes by water hyacinth roots, Bioresour. Technol., 52 (1995) 79–83.
[56] F.T. Li, H. Yang, Y. Zhao, R. Xu, Novel modified pectin for heavy metal adsorption, Chin. Chem. Lett., 18 (2007) 325–328.
[57] G. Crini, Recent developments in polysaccharide-based materials used as adsorbents in wastewater treatment, Prog. Polym. Sci., 30 (2005) 38–70.